Statistical analysis of magnetically soft particles in magnetorheological elastomers

You may also be interested in:

Statistical analysis of magnetically soft particles in magnetorheological elastomers

T Gundermann[1], P Cremer[2], H Löwen[2], A M Menzel[2] and S Odenbach[1]

[1] Technische Universität Dresden, Institute of Fluid Mechanics, D-01062, Dresden, Germany
[2] Heinrich-Heine-Universität Düsseldorf, Institut für Theoretische Physik II: Weiche Materie, D-40225 Düsseldorf, Germany

E-mail: thomas.gundermann@tu-dresden.de

Abstract

The physical properties of magnetorheological elastomers (MRE) are a complex issue and can be influenced and controlled in many ways, e.g. by applying a magnetic field, by external mechanical stimuli, or by an electric potential. In general, the response of MRE materials to these stimuli is crucially dependent on the distribution of the magnetic particles inside the elastomer. Specific knowledge of the interactions between particles or particle clusters is of high relevance for understanding the macroscopic rheological properties and provides an important input for theoretical calculations. In order to gain a better insight into the correlation between the macroscopic effects and microstructure and to generate a database for theoretical analysis, x-ray micro-computed tomography (X-μCT) investigations as a base for a statistical analysis of the particle configurations were carried out. Different MREs with quantities of 2–15 wt% (0.27–2.3 vol%) of iron powder and different allocations of the particles inside the matrix were prepared. The X-μCT results were edited by an image processing software regarding the geometrical properties of the particles with and without the influence of an external magnetic field. Pair correlation functions for the positions of the particles inside the elastomer were calculated to statistically characterize the distributions of the particles in the samples.

Supplementary material for this article is available online

(Some figures may appear in colour only in the online journal)

1. Introduction

Magnetorheological elastomers (MRE) are an interesting class of actively controllable smart materials. They consist of magnetic particles embedded into an elastic polymer matrix [1–4]. This combination of materials allows to dynamically influence many material properties simply by applying an external magnetic field, opening the way for a wide range of applications in technology [5–15]. The magnetic particles are usually made of a ferromagnetic material, e.g., carbonyl-iron powder [10–15] or neodymium-iron-boron [16] in a size range of a few nanometers up to several micrometers. To generate the polymeric matrices, polydimethylsiloxane (PDMS) or poly(N-isopropylacrylamide) is frequently used.

Applying a magnetic field to such a kind of MRE, internal magnetodipolar forces can cause changes in static and dynamic properties [17–24]. Structurally, during synthesis, these forces can lead to a rearrangement of the particles towards chain-like aggregates oriented parallel to the direction of the applied magnetic field [25–28]. Inducing these forces in the final product, counteracting elastic restoring forces by the surrounding matrix oppose to the reorganization. The magnitudes of the magnetodipolar forces are largely dependent on the distribution of the particles inside the matrix, particularly on the distance between neighboring particles.

During the last years, a noninvasive method for the three-dimensional investigation of the morphology of materials

using x-ray micro-computed tomography (X-μCT) was developed [29–31]. This measuring technique enables a quantitative analysis of the geometrical properties of single particles in MRE materials. It is possible to perform X-μCT investigations under the influence of an external magnetic field by implementing a magnetic field setup into the CT-system [31, 32].

The main interest of the current study is to observe and analyze the particle distribution within different samples. We have investigated isotropic samples with and without exposure to an external magnetic field during measurement. Samples with an already imprinted chain structure (anisotropic samples) due to initial polymerization under the influence of an external magnetic field are addressed as well. The initially isotropic samples show a formation of small chain-like aggregates when applying an external magnetic field. Consequently, there is a structural difference between the cases with and without an external magnetic field switched on [32]. For both cases, pair correlation functions (PCF) are calculated and compared to the situation in the anisotropic samples, where chain-like aggregates are always present. These PCF are of interest as an input for statistical theories, see also their previous use in the characterization of dipolar liquids [33–40].

The experimental samples were based on magnetically soft iron particles with a mean diameter of about 45 μm and a particle content of 2, 5, 10, and 15 wt% which corresponds to 0.27, 0.70, 1.47, and 2.32 vol%, respectively. These particles were embedded into a PDMS matrix supplied by Wacker Chemie AG (Germany). Applying the external magnetic field was achieved by two permanent magnets in the X-μCT system that create an external homogeneous magnetic flux density of approximately $B = 270$ mT [31].

2. Experimental

2.1. Setup

To carry out the investigations we used an X-μCT system based on a nano-focus tube with a maximum acceleration voltage of 160 kV, a movable sample holder with two cylindrical permanent magnets to adjust the magnetic field, and a detector with a photodiode array of 2000 $\times$ 2048 (vertical $\times$ horizontal) pixels [29–31]. The permanent magnets were mounted in a displaceable fashion and could generate a homogeneous magnetic field parallel to the direction of gravity in the range of $B = 0-270$ mT. This enables investigations of cylindrical regions of 4 mm both in height and in diameter, within a magnetic field with a degree of homogeneity of 97% in radial and 94% in axial direction [31]. More details on the measuring setup can be found in [31, 32].

During the CT investigations, the temperature was kept constant at 20 °C. The projection images in the experiments were generated by rotating the sample with 0.25° angular increment for a tube current of 170 μA and an acceleration voltage of 90 kV. The exposure time was varied between 2

and 6.5 s to achieve a suitable image quality. The magnification was 15, which resulted in a resolution of 1 pixel = 3.2 μm. CT-reconstruction was carried out using a home-made software.

2.2. Samples

Our samples were of cylindrical shape of diameter $d = 3.5$ mm and height $h = 3.5$ mm. The polymer host matrix was prepared from the elastomer kit Elastosil® RT 745 A/B, provided by Wacker Chemie AG Germany. Elastosil is a two-component silicon with a curing agent in one of the two components. The components were mixed in a mass ratio of 1:1. After mixing the components, a highly viscous silicon oil of viscosity $\eta = 100$ Pas (at 23 °C), produced by Wacker Chemie AG (Germany), was added as a softener in a content ratio of 60 wt% related to the two silicon components. This softener leads to an adjustment of the elastic moduli of the polymer matrix and to a reduction of the sedimentation rate due to gravitation. After mixing the components and the softener, magnetically soft iron powder ASC200, supplied by Höganäs AB (Sweden), was added. The average particle size was approximately 45 μm. Further details about the particle size distribution can be found in [29].

To investigate the statistical particle distribution in MREs, different samples with particle contents of 2, 5, 10, and 15 wt% (0.27, 0.70, 1.47, 2.32 vol%, respectively) were produced. Samples with isotropic particle distributions were synthesized by pouring the final mixture (with particles added) into a mold that was then placed into a 95 °C water bath for 2 h to guarantee the polymerization of the samples. Samples with anisotropic particle distributions were produced by exposing the final mixture to a homogeneous magnetic field of $B = 270$ mT generated by a laboratory electronic magnet from the company Bruker Corp. (Germany) during polymerization. Again, the specified time for the sample polymerization amounted to 2 h at a temperature of 95 °C.

After preparation of the samples, CT-scans were performed. We anticipated a particle rearrangement upon application of an external magnetic field [32]. Therefore, each sample was investigated in the absence and the presence of an external magnetic field. In this process, it was found that the particles within the anisotropic samples already featuring chain-like aggregates do not show significant rearrangement when the magnetic field is applied parallel to the chain structures. Thus, the cases we discuss in the following are isotropic samples at $B = 0$, isotropic samples at $B = 270$ mT, and anisotropic samples at $B = 0$. Example tomograms of the samples with different particle distributions are shown in figures 1(a) and (b).

3. Evaluation

A quantitative analysis identifying single particles inside the elastomeric matrices becomes possible by evaluating the reconstructed tomographic scans with an image processing
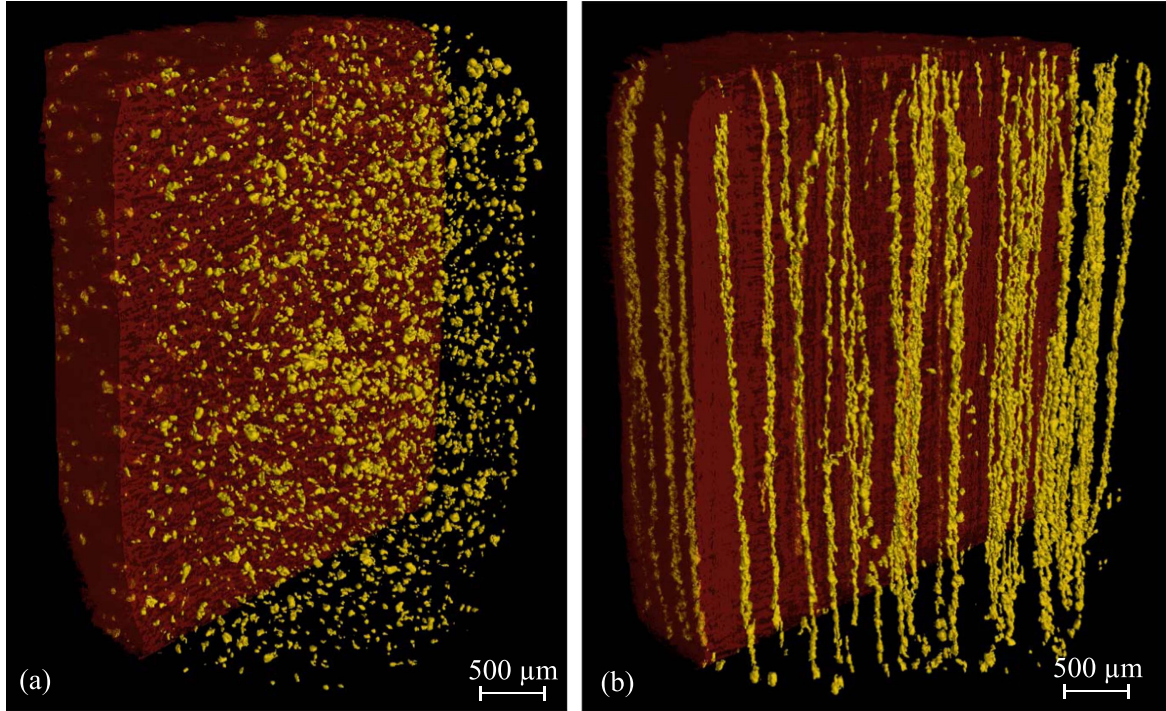
Figure 1. Tomograms of cylindrical MRE samples of 5 wt% particle content with (a) isotropic structure in the absence of an external magnetic field. The anisotropic sample (b) was generated by applying an external magnetic field in axial direction during the polymerization process. The host matrix is shown in dark red (dark gray) and the particles in yellow (light gray).

software. For the quantitative analysis, the software MATLAB 7.10.0 with the image toolbox DIPimage was used. Due to a lower absorption coefficient of the elastomer relatively to the particles, the matrix in figure 1 (in dark red/ dark gray) can be distinguished from the particles (in yellow/ light gray). A threshold criterion based on the gray value in the tomographic data was used to separate the particles from the matrix. After separation of the components, individual particles in clusters were identified (segmented) using a watershed algorithm [41]. To avoid an incorrect separation of the particles, it was important to adjust the parameters of the watershed algorithm. To guarantee an accurate particle segmentation, the threshold criterion and the watershed algorithm were calibrated to the size distribution of the magnetic particles obtained by a laser diffraction method. Figure 2 illustrates a segmented cluster of particles within an anisotropic sample for a particle content of 5 wt%.

After segmentation of the clustered particles, the particles were labeled and their size and center coordinates were determined and organized into a database. The particle distribution was determined from this database. In a homogeneous sample, a useful approach to statistically characterize the distribution of particles is to consider the PCF [42, 43]

$$g(\mathbf{r}) = \frac{V}{N^2} \left\langle \sum_i \sum_{j \neq i} \delta(\mathbf{r} - (\mathbf{r}_j - \mathbf{r}_i)) \right\rangle, \quad (1)$$

where N is the number of particles, V is the sample volume, $\mathbf{r}_i = (x_i, y_i, z_i)$ and $\mathbf{r}_j = (x_j, y_j, z_j)$ denote the positions of particles i and j, respectively, δ is the Dirac delta function,

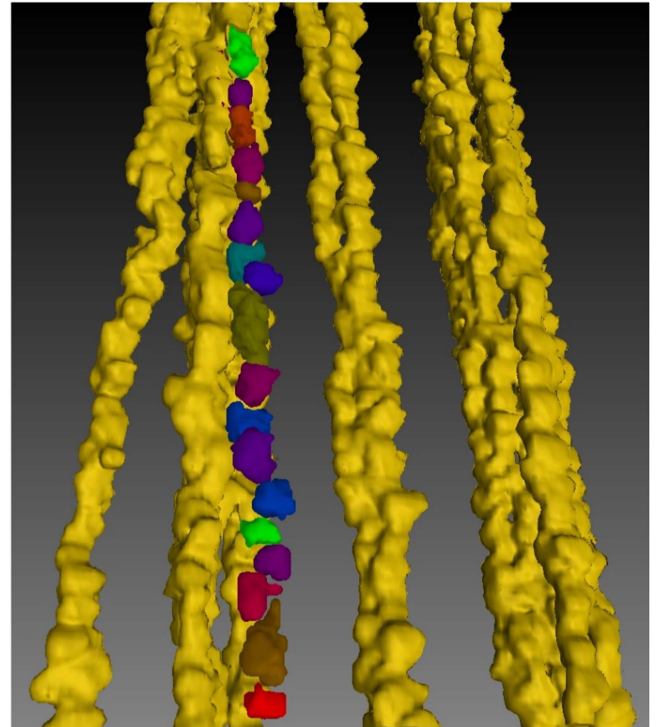**Figure 2.** Segmented individual particles in one chain of an anisotropic MRE sample with a particle content of 5 wt% as opposed to the still non-segmented particles in the other chain structures.

and $\langle \cdot \rangle$ denotes an ensemble average. The PCF is proportional to the probability density for finding a pair of particles in the sample at a separation as given by the vector $\mathbf{r}$. In an ideal gas

of particle density N/V, where the ensemble-averaged distribution of particles is uniform, this probability density is given by $(N/V)^2$. So $g(\mathbf{r})$ relates the actual nonuniform distribution to the uniform ideal-gas distribution. For very short distances smaller than the finite particle size, $g(\mathbf{r}) = 0$ because the rigid particles cannot interpenetrate. At very long distances, there is no correlation between two particles anymore so that the probability density to find a particle at a separation $\mathbf{r}$ from another particle becomes uniform as for the ideal gas and $g(\mathbf{r}) = 1$.

Our anisotropic samples were produced in an external magnetic field parallel to the cylinder axis ($\hat{\mathbf{z}}$-direction). Moreover, our isotropic samples were probed under the influence of an equally oriented magnetic field. These samples possess a cylindrical symmetry and, therefore, the probability density to find a particle pair at a certain separation only depends on the particle distances $r_{\parallel}$ in the axial direction and $r_{\perp}$ perpendicular to it. That means a PCF of only two variables given by

$$g(r_{\parallel}, r_{\perp}) = \frac{V}{4\pi r_{\perp} N^2} \left\langle \sum_i \sum_{j \neq i} \delta(r_{\parallel} - |z_j - z_i|) \right.$$
$$\left. \times \delta\left(r_{\perp} - \sqrt{(x_j - x_i)^2 + (y_j - y_i)^2}\right) \right\rangle \quad (2)$$

contains the same information as $g(\mathbf{r})$ and can be termed cylindrical distribution function. For the analysis of the isotropic samples in the absence of an external field we can proceed one step further and consider the radial distribution function

$$g(r) = \frac{V}{4\pi r^2 N^2} \left\langle \sum_i \sum_{j \neq i} \delta(r - |\mathbf{r}_j - \mathbf{r}_i|) \right\rangle \quad (3)$$

with $r := |\mathbf{r}|$. See the supplemental material available online at stacks.iop.org/SMS/26/045012/mmedia for a detailed discussion on why equations (2) and (3) are equivalent to equation (1) when the particle distribution features cylindrical symmetry or is isotropic, respectively.

In practice, the computation of $g(r)$ was performed in the following way. The possible values for the distance r are sorted into n discrete bins of thickness Δr with possible distance values $r_k = (k + 1/2)\Delta r$, where $k \in \{0, \dots, n - 1\}$. A histogram of the occurrences of particle distance is computed. The occupation number of the kth bin is incremented whenever $|\mathbf{r}_j - \mathbf{r}_i| \in [k\Delta r, (k + 1)\Delta r[$. This procedure reflects the sum of δ-distributions in equation (3). Since each bin represents a spherical shell of finite thickness Δr, the normalization by $4\pi r^2$ is replaced with the normalization by $\frac{4}{3}\pi((k + 1)^3 - k^3)(\Delta r)^3$. However, our samples are finite, so there is one complication here. Let b_i be the distance of particle i to the sample boundary. If the interparticle distance $|\mathbf{r}_j - \mathbf{r}_i|$ would fall into a bin, but $b_i < |\mathbf{r}_j - \mathbf{r}_i|$, the normalization becomes complicated because the spherical shell corresponding to the bin centered around $\mathbf{r}_i$ intersects with the boundary. We have circumvented this problem by only taking those pairs of particles into account for which $b_i \geqslant |\mathbf{r}_j - \mathbf{r}_i|$. But then a bin only gets the chance to

grow if $b_i \geqslant (k + 1)\Delta r$, the outer radius of the spherical shell. Therefore, one division by N in equation (3) has to be replaced with a division by the number of particles i for which $b_i \geqslant (k + 1)\Delta r$. To summarize, we have used the following formula for the calculation of the radial distribution function

$$g(r_k) \approx \frac{V}{N}$$
$$\times \left\langle \frac{\sum_i \sum_{j \neq i} 1_{[k\Delta r, (k+1)\Delta r[}(|\mathbf{r}_j - \mathbf{r}_i|) 1_{[0, b_i]}(|\mathbf{r}_j - \mathbf{r}_i|)}{\frac{4}{3}\pi((k + 1)^3 - k^3)(\Delta r)^3 \sum_i 1_{[(k+1)\Delta r, \infty[}(b_i)} \right\rangle,$$
$$1_{[a, b[}(x) = \begin{cases} 1 & \text{for} \quad x \in [a, b[, \\ 0 & \text{else.} \end{cases} \quad (4)$$

The calculation of the cylindrical distribution function $g(r_{\parallel}, r_{\perp})$ was performed in an analogous fashion. Here, both distances $r_{\parallel}, r_{\perp}$ have to be discretized. Bins represent cylindrical shells with discretized radii and heights and again count the number of times a separation $|\mathbf{r}_j - \mathbf{r}_i|$ falls within their shell. Also the same considerations for the sample boundary apply.

In evaluating the statistics for our experimental systems, the averages were performed for each individual sample separately. For this purpose, sufficiently homogeneous regions were identified as described in the following.

4. Results

4.1. Statistical analysis of MREs with isotropic particle distribution

First, we had to make sure that the requirement of the homogeneity of the sample is sufficiently met. The criterion was based on the homogeneity of the particle number density within the sample. Imagine around the geometrical center of our cylindrical sample a smaller cylinder of height H and radius R. If the particle number density $\rho(H, R)$ within the enclosed volume is a sufficiently constant function of H and R, then the sample can be regarded as homogeneous. As an example, we plot in figure 3 for an isotropic sample with a particle content of 15 wt% the particle density $\rho(H, R = 1.5 \text{ mm})$ within a cylinder of variable height and fixed radius as well as $\rho(H = 3.0 \text{ mm}, R)$ within a cylinder of fixed height and variable radius. While the former shows stronger fluctuations, especially for large H before the full sample height is reached, the latter remains relatively constant up to the full radius of the sample. The spikes at very low radii and heights are due to the poor statistics when only a few particles fit into the cylinder. The significant decrease at high values of H and R is to some extent due to slight deviations of the sample from a perfect cylindrical shape, which is also visible in figure 1. When the test cylinders that are fitted into the sample for our evaluation reach the overall extent of the sample, these shape irregularities become important. If voids are included in the probe volume, the density drops. We therefore chose a maximum height $H_m = 3.0 \text{ mm}$ and radius
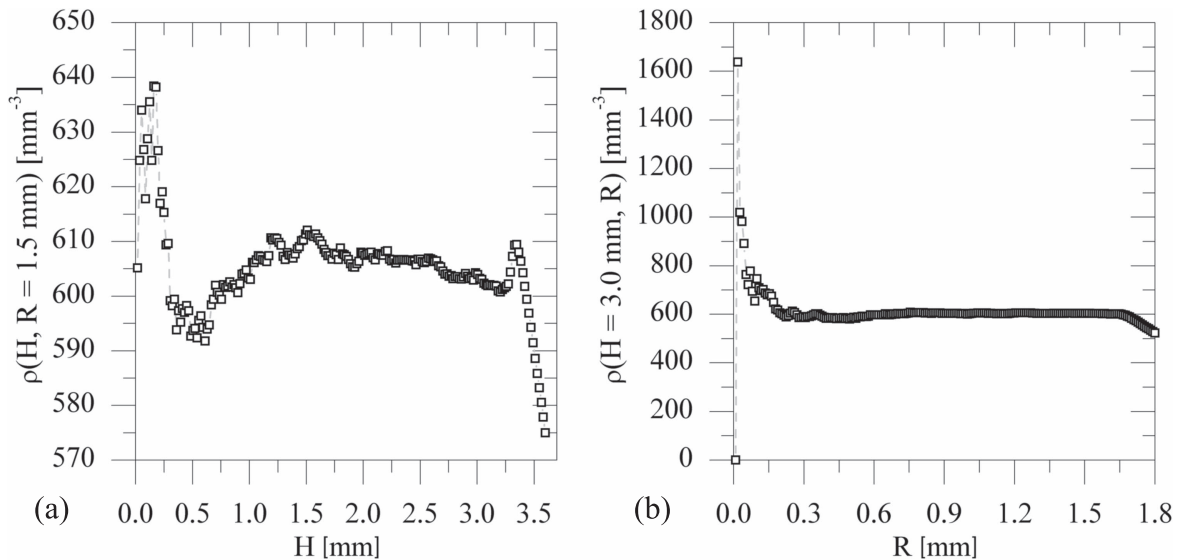
Figure 3. Particle number density $\rho(H, R)$ within a cylinder of height H and radius R centered around the geometrical center of an isotropic sample with a particle content of 15 wt%. (a) When the cylinder radius is kept fixed at $R = 1.5$ mm and its height is varied, the particle density $\rho(H, R = 1.5$ mm$)$ shows some fluctuations, indicating that the sample is not perfectly homogeneous in the axial direction, especially when going beyond $H = 3.0$ mm. (b) When the height is kept fixed and the radius is varied, the particle number density $\rho(H = 3.0$ mm, $R)$ shows less fluctuations, up to at least $R = 1.5$ mm. Since the sample shape slightly deviates from that of a perfect cylinder, here is a significant decrease for both $\rho(H > 3.2$ mm, $R)$ and $\rho(H, R > 1.6$ mm$)$ when the test cylinder reaches the overall extent of the sample and voids are included in the evaluation.

$R_m = 1.5$ mm and only used the enclosed sample volume in our calculations.

After determining a sample region that is approximately homogeneous, we calculated the radial distribution function. The results are shown in figure 4. For small interparticle distances we have $g(r) = 0$, because even the smallest particles in the sample show a finite separation distance between their centers. Starting with $r \approx 20$ μm, $g(r)$ rapidly increases as more and more configurations become possible where also particles of larger size do not overlap. Saturation is already reached at $r \approx 70$ μm. This represents a reasonable value, considering the mean particle diameter of approximately 45 μm. From there on $g(r)$ remains at a constant level of 1. Our results suggest that mainly approximate repulsive hard-sphere-like interactions between the particles determine the particle arrangement in the sample. If this is the case, almost the same radial distribution function should be recovered when the same particles are redistributed in a random and non-intersecting way. We performed this test by generating artificial statistical ensembles of hard spheres within the same overall volume and with the same distribution of volumes of the individual particles as extracted from the real sample. The protocol is the following. For each particle in the real sample, we generate a spherical particle of identical volume. Then we insert this particle into the available sample volume, one at a time. During each event of insertion, the corresponding particle is placed at a random position, avoiding overlap with previously placed spheres. If there is any overlap with any previously inserted particle, a new random position is generated, otherwise we proceed to the next particle, and so on. When all particles are inserted, the result is an isotropic distribution of hard spheres that have the same volume
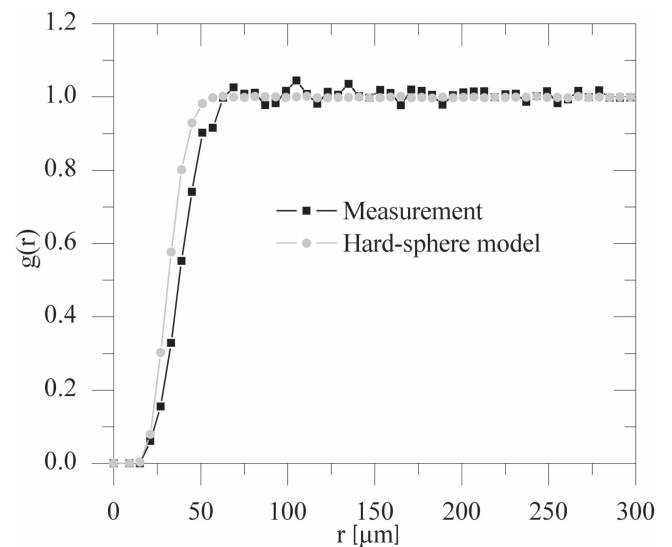

Figure 4. Radial distribution function for the isotropic sample with a particle content of 15 wt% and vanishing magnetic field. The data are in agreement with the results from a polydisperse hard-sphere model where all particles are transformed into spheres, keeping their volumes as determined experimentally and then randomly distributing them. This suggests that repulsive hard-core-like interactions dominate the particle arrangement during the preparation process of the sample.

distribution as the particles in the real experimental sample. 100 of these artificial distributions were created and the resulting radial distribution functions were averaged. The distribution function obtained from this polydisperse hard-sphere model is plotted in figure 4 and shows reasonable qualitative agreement with the real sample. Isotropic samples
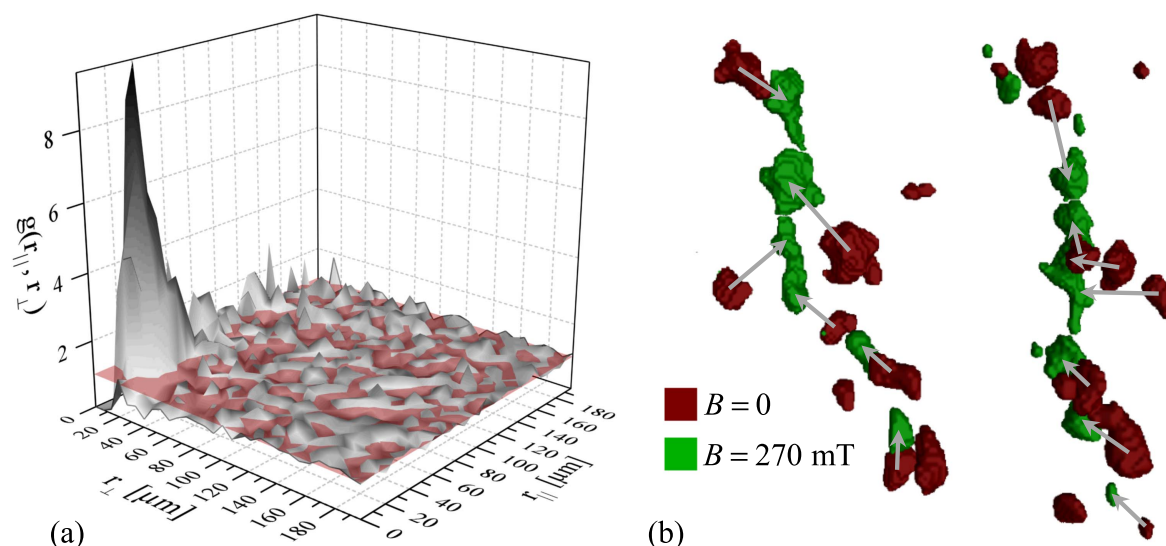
Figure 5. (a) Cylindrical distribution function $g(r_{||}, r_{\perp})$ for the isotropic sample with a particle content of 15 wt% under the influence of an external magnetic field of $B = 270$ mT. There is a pronounced peak in the direction parallel to the external field, indicating that the particles prefer to have their neighbors in a direction along the external field. Since this peak is absent in the absence of an external magnetic field, it indicates internal rearrangement upon field application. The radial direction $g(r_{||} = 0, r_{\perp})$ is mostly featureless. (b) Tomographic scan to visualize the chain formation when an external magnetic field is applied to the initially isotropic sample. These data were obtained in the same way as described in [32].

with a lower particle content lead to very similar results, albeit with worse statistics due the lower total number of particles.

The situation changed when an external magnetic field of $B = 270$ mT was applied to the sample in axial direction when measuring the particle distribution. In figure 5(a) we illustrate the cylindrical distribution function $g(r_{||}, r_{\perp})$. While no significant structure of $g(r_{||}, r_{\perp})$ is observed in the direction perpendicular to the field, there is a strongly increased probability for each particle to find another one in close vicinity in the parallel direction. In particular, there is a peak at $r_{\perp} \approx 0$ and $r_{||} \approx 45$ μm. The latter distance corresponds to the mean particle diameter within our samples. Beyond this peak, however, the correlation rapidly decays and there are no striking features anymore. These observations are in agreement with the picture of magnetic particles attracting each other along the external field direction. The attraction seems to be strong enough to put the particles close to contact in spite of the counteracting forces generated by a deformed matrix environment, see figure 5(b). This is in agreement with the picture of chains of magnetic particles forming in the sample under the influence of the external magnetic field [21]. However, higher-order correlation peaks are not clearly identified, possibly due to the relatively low particle content, due to the elastic interactions preventing particles from moving too far, and due to the polydispersity of the particles.

Since the PCF does not contain any direct statement on the number of particles in a chain, a database searching algorithm was developed to determine this number. For this purpose, a cylinder with $R = 25$ μm and $H = 400$ μm was defined around each particle. Each particle that was found inside this cylinder with a center-to-center distance from the initial particle smaller than the sum of the two particle diameters is defined to belong to the same chain. After the assignment, the number of particles organized in chains of a
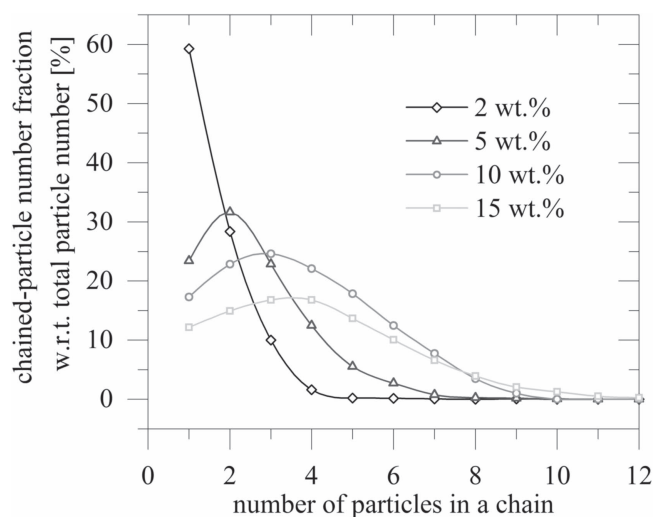

Figure 6. Numbers of particles organized in chains of given size for different particle contents. The chains formed in the isotropic samples when a magnetic field of $B = 270$ mT was applied. Their average size increases with increasing particle content.

given size were determined and are plotted in figure 6 for the different particle quantities. We observed that the lengths of the chains increase with increasing particle content.

4.2. Statistical analysis of MREs with anisotropic particle distribution

As already shown in figure 1, the anisotropic samples created by applying an external magnetic field during the polymerization process feature chain-like aggregates in the direction of the originally applied field. These chains span the entire sample from bottom to top. It has previously been observed that the structure of chains in anisotropic MREs
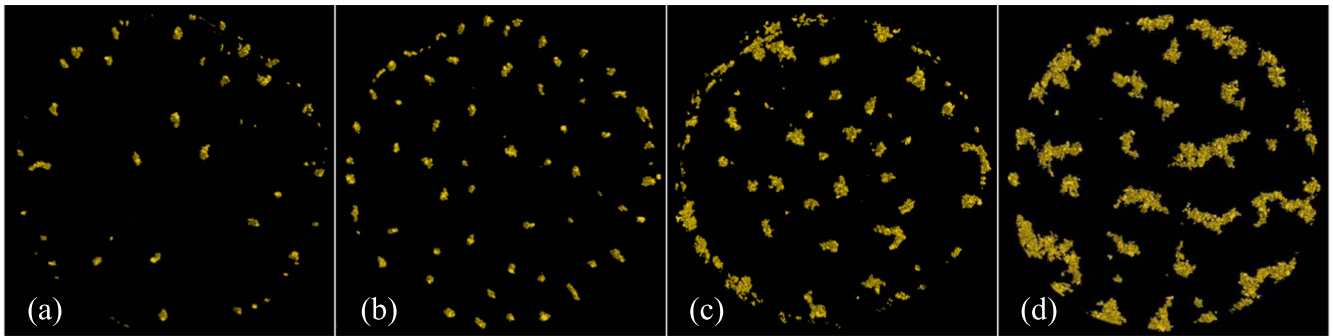
Figure 7. Tomographic results for the horizontal cross-sections through the center of the anisotropic samples with particle contents of (a) 2 wt%, (b) 5 wt%, (c) 10 wt%, and (d) 15 wt%.
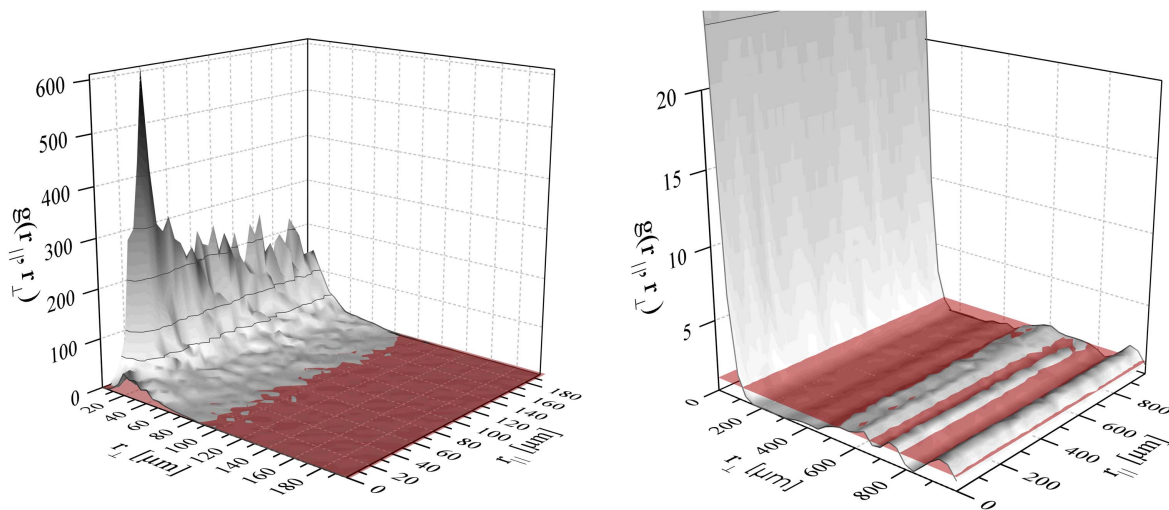

Figure 8. Two different illustrations of the cylindrical distribution function $g(r_\parallel, r_\perp)$ for an anisotropic sample with a particle content of 2 wt%. The left plot illustrates the behavior for smaller separation distances. There is a pronounced peak at low $r_\perp$, which reflects the preferred nearest-neighbor positioning along the axial direction. The correlations in this direction are overall very high and decay slowly. Contrary to that, in the perpendicular direction there are no striking features and the correlation is lost very quickly. The right plot aims to demonstrate the correlations between separate chains. For long distances $r_\perp$, there is first a depleted region corresponding to the voids between separate chains. After that, however, there is a series of peaks reflecting the positioning of neighboring chains.

typically depends on the particle content [29]. This is also the case for our anisotropic samples. We illustrate horizontal cross-sections through our samples with different particle content in figure 7, where the structural changes with increasing particle content are evident. At low particle content of 2 wt%, the chains are thin and orientated in the direction along the magnetic field initially applied during polymerization. With increasing particle content, the structures begin to thicken and to expand in the direction perpendicular to the magnetic field (figure 7(d)). Obviously, in the directions perpendicular to the anisotropy axis, the particles are not distributed uniformly. Instead, they rather appear to be clustered at certain mutual distances. Such inhomogeneous distributions are known to be able to significantly affect the mechanical response [44].

Again we determined the cylindrical distribution functions. Results for particle contents of 2 and 15 wt% are plotted in figures 8 and 9, respectively. There are obviously huge differences between the directions parallel and perpendicular to the anisotropy axis. Along the direction of the chains the correlation is much stronger and long-ranged, especially for

the samples with low particle content. In both samples, there is again a peak at $r_\parallel \approx 45\ \mu$m, $r_\perp \approx 0$ identifying nearest-neighboring particles in the axial direction. In the direction perpendicular to the chains, the correlations are lost much more quickly, especially for the 2 wt% sample. In contrast to that, the sample with 15 wt% particle content features chains of larger thickness in the perpendicular directions, so that the correlations in these directions decay much more slowly. At long distances in the perpendicular direction, we can first observe a depleted region where the probability to find other particles becomes very low and $g(r_\parallel, r_\perp)$ almost vanishes. Beyond this depleted region, the values increase again and indicate the presence of other chains. This manifests itself as a series of discrete peaks at $r_\perp \geqslant 500\ \mu$m in the sample with low particle content and as one smeared-out peak in the sample with high particle content. In figure 10 this is illustrated more clearly and also for the other particle contents. There we plot the cylindrical distribution function $g(r_\parallel = 0, r_\perp)$ only as a function of the perpendicular distance, setting the distance in the axial direction to zero.
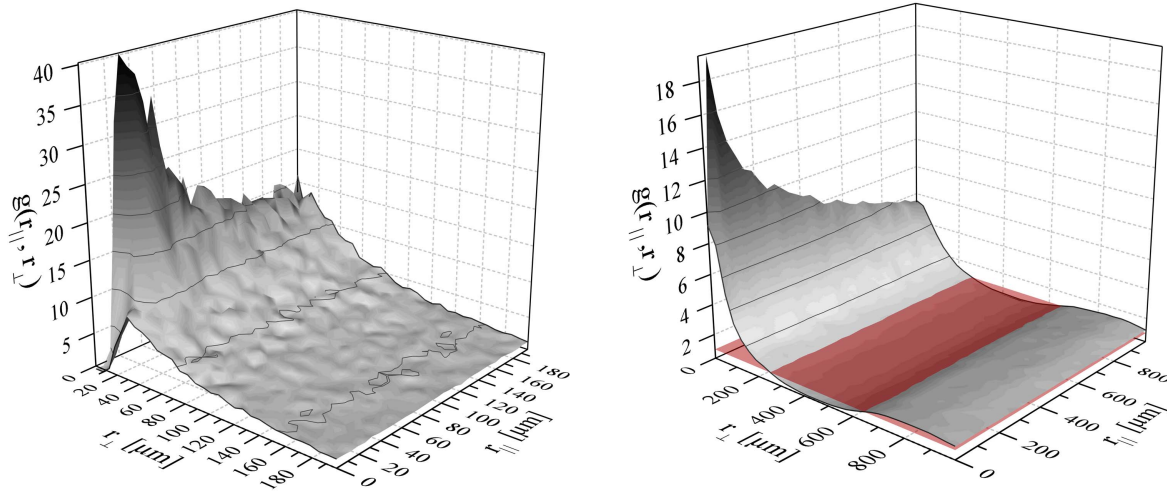
Figure 9. Same as figure 8 but for a particle content of 15 wt%. The chains in these systems are typically much thicker and less ordered. Thus, compared to the particle content of 2 wt% there is less correlation between particles along the chains but more in the directions perpendicular to the chain axes. For long distances in the perpendicular directions there is again a depleted area where $g(r_\parallel, r_\perp)$ drops close to zero. Beyond this depletion zone one smeared-out peak reflects the positioning of neighboring chains.
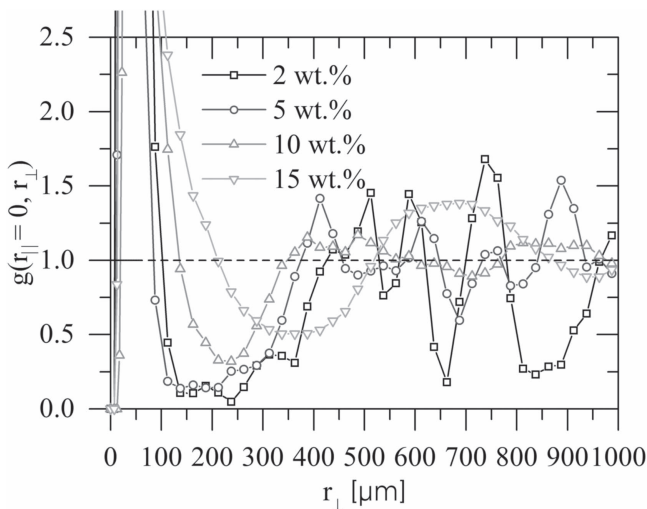

Figure 10. Cylindrical distribution functions $g(r_\parallel = 0, r_\perp)$ of anisotropic samples for different particle contents, where only $r_\perp$ is varied and $r_\parallel$ is set to zero. This plot illustrates more clearly the correlations between separate chains and the depleted region due to the voids between the chains where it is very unlikely to encounter another particle.

To further quantify the correlations between the particle chains, we also performed an analysis using a Delaunay triangulation method [29, 45]. First, for different cross-sectional planes, see figure 7, the centers of the chains were detected. Using Delaunay triangulation, each plane was tessellated into triangles with their vertices located in the chain centers. The distances between the chains were then determined as the lengths of the edges of these triangles.

An example for the resulting distributions is shown in figure 11(a) for a particle content of 15 wt%. Approximately, the distances between the particle chains follow a Gaussian distribution. Extracting the average chain separation distance, we found for our samples that the chain distances first decrease from the 2 wt% to the 5 wt% case, see figure 11(b).

For the higher particle contents of 10 and 15 wt%, we then observed both the chain separation distances and the chain thicknesses to increase. This behavior is connected to the dependence of the total number of chains on the particle content. For the particle content of 5 wt%, the chains still remain thin and aligned, as already shown in figure 7. When the particle content is further increased, the chains start to expand in the direction perpendicular to the magnetic field. This leads to a decreasing number of chains and, therefore, to an increase in chain distance.

5. Summary

This work demonstrates the possibility to extract and quantify particle distributions within MRE via X-μCT tomographic measurements. A statistical analysis of these distributions leads to insights into the particle interactions within such materials. X-μCT provides a method to detect individual particles inside these systems and to track their rearrangement when an external stimulus is applied. In a measured tomogram, particles are still clustered and not individually visible. By using methods of digital image evaluation, clustered particles can be distinguished. This provides the possibility to analyze their geometrical properties and to generate a database for statistical processing. From the database, PCF characterizing the particle arrangements were calculated. Several different experimental samples were produced in this work, all of them consisting of particles of carbonyl-iron powder embedded into a polymeric matrix made of PDMS. Isotropic and anisotropic samples were synthesized with particle contents of 2, 5, 10, and 15 wt%. The anisotropic samples were created by applying a magnetic field during the polymerization process, which led to the formation of chains along the field direction. For the isotropic samples, tomographic studies with and without an external magnetic field of $B = 270$ mT applied during data collection have been carried out. The
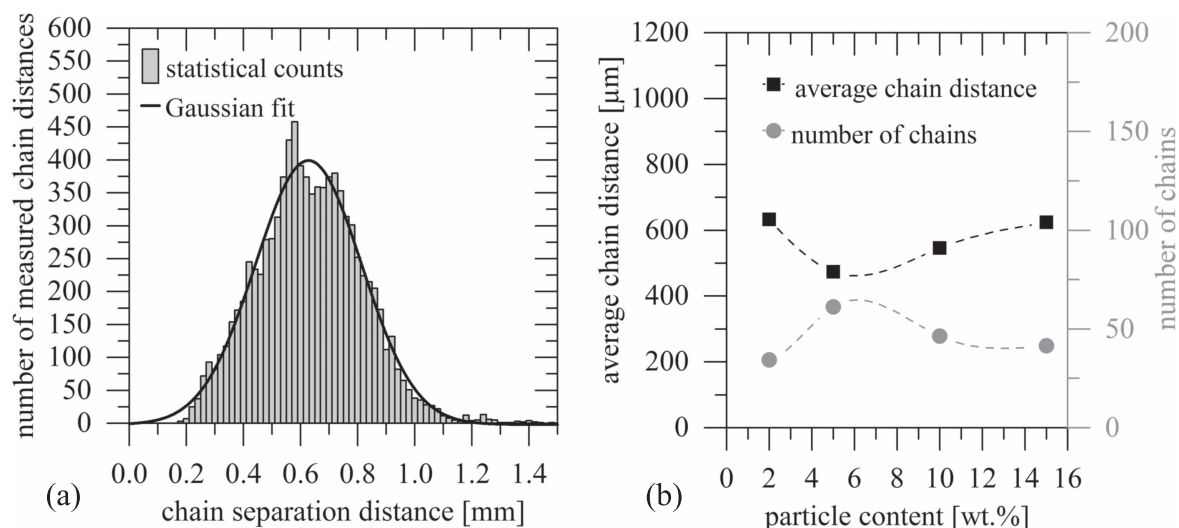
Figure 11. (a) Histogram of the distances between particle chains obtained from the Delaunay triangulation for a particle content of 15 wt%. The chain distances obviously follow a Gaussian distribution, from which an average chain distance can be extracted. (b) Plots of the average chain distances and the number of chains for all considered particle contents.

analysis of the PCF for these isotropic samples indicated the absence of structures in the absence of external magnetic fields. When an external magnetic field is applied, the nearest particle neighbors are most likely found along the magnetic field direction as the particles attract each other along this direction. Apparently, smaller chain-like structures are formed under the influence of the external field in the isotropic samples. However, larger anisotropic structures seem to rarely emerge. The tomographic measurements on the anisotropic samples were carried out without an external magnetic field applied during data acquisition, because the field did not significantly alter the structures. We characterized the morphology of the chain-like aggregates in these anisotropic samples by determining corresponding PCF. The chain morphology strongly depends on the particle content of the samples. An increasing particle content leads to increased chain thicknesses perpendicular to the magnetic field. Furthermore, we were able to address correlations in the positioning of separate chains.

In summary, a tool was described to characterize the distribution of particles in particle-matrix systems. In the future, measurements on samples with higher particle contents should be performed. Also the statistics for the calculation of the PCF can be improved by combining the tomographic results of more samples. The obtained correlation functions can then be used as an input for statistical theories. Moreover, measurements on samples with still higher particle contents and, additionally, measurements on anisotropic samples exposed to an external magnetic field perpendicular to the chain axes should be performed.

Acknowledgments

References

[1] Zrinyi M, Barsi L and Büki A 1997 *Polym. Gels Netw.* **5** 415
[2] Odenbach S 2016 *Arch. Appl. Mech.* **86** 269
[3] Menzel A M 2015 *Phys. Rep.* **554** 1
[4] Filipcsei G, Csetneki I, Szilágyi A and Zrínyi M 2007 *Adv. Polym. Sci.* **206** 137
[5] Varga Z, Filipcsei G and Zrinyi M 2006 *Polymer* **47** 227
[6] Fu J, Yu M, Dong X M and Zhu L X 2013 *J. Phys.: Conf. Ser.* **412** 012032
[7] Jolly M R, Carlson J D, Muñoz B C and Bullions T A 1996 *J. Intell. Mater. Sys. Struct.* **7** 613
[8] Ginder J, Nichols M, Elie L and Tardiff J 1999 *Proc. SPIE* **3675** 131
[9] Jarkova E, Pleiner H, Müller H-W and Brand H R 2003 *Phys. Rev.* E **68** 041706
[10] Deng H-X, Gong X-l and Wang L-h 2006 *Smart Mater. Struct.* **15** N111
[11] Sun T, Gong X, Jiang W, Li J, Xu Z and Li W 2008 *Polym. Test.* **27** 520
[12] Mitsumata T, Ohori S, Honda A and Kawai M 2013 *Soft Matter* **9** 904
[13] Stoll A, Meyer M, Monkman G J and Shamonin M J 2014 *J. Appl. Polym. Sci.* **131** 39793
[14] Schubert G and Harrison P 2016 *Smart Mater. Struct.* **25** 015015
[15] Wang Y, Xuan S, Dong B, Xu F and Gong X 2016 *Smart Mater. Struct.* **25** 025003
[16] Kramarenko E Y, Certovich A V, Stepanov G V, Semisalova A S, Makarova L A, Perov N S and Khokhlov A R 2015 *Smart Mater. Struct.* **24** 035002
[17] Pessot G, Cremer P, Borin D Y, Odenbach S, Löwen H and Menzel A M 2014 *J. Chem. Phys.* **141** 124904
[18] Tarama M, Cremer P, Borin D Y, Odenbach S, Löwen H and Menzel A M 2014 *Phys. Rev.* E **90** 042311
[19] Cremer P, Löwen H and Menzel A M 2015 *Appl. Phys. Lett.* **107** 171903
[20] Huang S, Pessot G, Cremer P, Weeber R, Holm C, Nowak J, Odenbach S, Menzel A M and Auernhammer G K 2016 *Soft Matter* **12** 228
[21] Pessot G, Löwen H and Menzel A M 2016 *J. Chem. Phys.* **145** 104904
[22] Cremer P, Löwen H and Menzel A M 2016 *Phys. Chem. Chem. Phys.* **18** 26670

[23] Biller A M, Stolbov O V and Raikher Y L 2014 *J. Optoelectron. Adv. Mater.* **17** 1106

[24] Weeber R, Kantorovich S and Holm C 2015 *J. Magn. Magn. Mater.* **383** 262

[25] Böse H 2007 *Int. J. Mod. Phys.* B **21** 4790

[26] Stepanov G, Borin D and Odenbach S 2009 *J. Phys.: Conf. Ser.* **149** 0120986

[27] Han Y, Hong W and Faidley L E 2013 *Int. J. Solids Struct.* **50** 2281

[28] Auernhammer G K, Collin D and Martinoty P 2006 *J. Chem. Phys.* **124** 204907

[29] Günther D, Borin D, Günther S and Odenbach S 2012 *Smart Mater. Struct.* **21** 015005

[30] Borbath T, Günther S, Borin D, Gundermann T and Odenbach S 2012 *Smart Mater. Struct.* **21** 105018

[31] Gundermann T, Günther S, Borin D and Odenbach S 2013 *J. Phys.: Conf. Ser.* **412** 012027

[32] Gundermann T and Odenbach S 2014 *Smart Mater. Struct.* **23** 105013

[33] Rushbrooke G S, Stell G and Høye J S 1973 *Mol. Phys.* **26** 1199

[34] Joslin C G, Gray C G and Gubbins K E 1985 *Mol. Phys.* **54** 1117

[35] Wei D, Patey G N and Perera A 1993 *Phys. Rev.* E **47** 506

[36] Groh B and Dietrich S 1994 *Phys. Rev. Lett.* **72** 2422

[37] Klapp S H L and Patey G N 2000 *J. Chem. Phys.* **112** 10949

[38] Klapp S H L 2005 *J. Phys.: Condens. Matter* **17** 0953

[39] Zubarev A Y and Isakova L Y 2000 *Phys. Rev.* E **61** 5415

[40] Smallenburg F, Vutukuri H R, Imhof A, van Blaaderen A and Dijkstra M 2012 *J. Phys.: Condens. Matter* **24** 464113

[41] Gonzalez R C, Eddins S L and Woods R E 2014 *Digital Image Processing Using MATLAB* (Englewood Cliffs, NJ: Prentice-Hall)

[42] Allen M and Tildesley D 1989 *Computer Simulation of Liquids* (Oxford: Clarendon)

[43] Gray C G and Gubbins K E 1984 *Theory of Molecular Fluids I: Fundamentals* (Oxford: Oxford University Press)

[44] Bilger N, Auslender F, Bornert M, Michel J-C, Moulinec H, Suquet P and Zaoui A 2005 *Int. J. Solids Struct.* **42** 517

[45] Hjelle Ø and Dæhlen M 2006 *Triangulations and Applications* (Berlin: Springer)